Acta Crystallographica Section D
Biological Crystallography
ISSN 0907-4449

Ultrahigh-resolution structure of high-potential iron–sulfur protein from *Thermochromatium tepidum*

Lijun Liu,[a] Terukazu Nogi,[a] Masayuki Kobayashi,[b] Tsunenori Nozawa[b] and Kunio Miki[a,c]*

[a]Department of Chemistry, Graduate School of Science, Kyoto University, Sakyo-ku, Kyoto 606-8502, Japan, [b]Department of Biomolecular Engineering, Graduate School of Engineering, Tohoku University, Aoba-ku, Sendai 980-8579, Japan, and [c]RIKEN Harima Institute/SPring-8, Koto 1-1-1, Mikazukicho, Sayo-gun, Hyogo 679-5148, Japan

Correspondence e-mail: miki@kuchem.kyoto-u.ac.jp

Received 13 December 2001
Accepted 8 April 2002

PDB Reference: HiPIP, 1iua, r1iuasf.

Crystals of the high-potential iron–sulfur protein (HiPIP) from *Thermochromatium tepidum* diffract X-rays to 0.80 Å using synchrotron radiation at 100 K. The crystal structure of this HiPIP was refined at this ultrahigh resolution with anisotropic temperature factors for all atoms to conventional crystallographic R factors of 0.092 and 0.101 for $F_o > 4\sigma(F_o)$ and all reflections, respectively. The present structure provides a more precise picture than the previous 1.5 Å structure and allows location of the positions of most H atoms. The structure revealed a partly hydrophobic cavity near the main hydrophobic area and a much larger inter-cluster approach distance (23.454 Å, the c constant of the unit cell) in the crystal packing than other types of HiPIPs. The structural features involved in the electron-transfer reaction of HiPIP are discussed.

1. Introduction

High-potential iron–sulfur proteins (HiPIPs) are a class of ferredoxin proteins that have a molecular weight in the range 6–10 kDa and contain an $[Fe_4S_4]$ cubane cluster (Kerfeld *et al.*, 1998). In many phototrophic eubacteria, HiPIPs exist abundantly in the periplasmic space and function as soluble electron-transfer carriers between the membrane-bound photosynthetic reaction centre and the cytochrome bc_1 complex (Bartsch, 1978). They utilize two cluster oxidation states, $[Fe_4S_4]^{2+}$ and $[Fe_4S_4]^{3+}$, operating over a wide range of relatively high reduction potentials from +450 to +50 mV (Carter *et al.*, 1972; Meyer *et al.*, 1983). In addition, HiPIPs from different species show a large variation in their primary structures, net overall charges and sizes (Rayment *et al.*, 1992).

HiPIPs are still of great interest as a number of fascinating questions remain unanswered with regard to the dominant factors governing their reduction potentials and intermolecular electron-transfer behaviour. Crystallographic studies have revealed the presence of a hydrophobic environment around the $[Fe_4S_4]$ cluster that is constructed of several conserved aromatic residues (Breiter *et al.*, 1991; Rayment *et al.*, 1992). Mutagenesis studies have identified the effect of these aromatic residues on the stability of the $[Fe_4S_4]^{3+/2+}$ redox couple by isolating the cluster from the solvent (Agarwal *et al.*, 1995; Soriano *et al.*, 1996). Rapid electron self-exchange behaviour observed by the EPR technique lent support to the hypothetical mechanism that dimerization through a flattened and relatively hydrophobic surface patch might be of primary importance in the intermolecular electron transfer (Couture *et al.*, 1999). Very recently, the five hydrogen bonds that are highly conserved between backbone amides and metal-bound ligands, as iden-

tified by previous structural studies, were shown to significantly affect the reduction potential (Low & Hill, 2000), in contrast to the observation that the number of these hydrogen bonds was not a determinant of the redox potential. A *K*-edge X-ray absorption spectroscopic study showed that the significant effect of the covalency of the metal–ligand bond of the cluster on the reduction potential was attributable to the extent of hydrogen bonding, particularly that to the bridging sulfides (Glaser *et al.*, 2001). Moreover, molecular-dynamics and theoretical studies based on crystal and solution structures have brought insight into the possible electron-transfer pathway and the large variations in reduction potentials that depend on the class of HiPIPs (Banci *et al.*, 1992). In spite of extensive crystallographic, spectroscopic, mutagenesis, chemical modification and theoretical studies of HiPIPs, it is still unclear which factors determine the reduction potentials and electron-transfer behaviour, since it is not easy to define how covalent bonds, hydrogen bonding and through-space jumping contribute to these behaviours (Balabin & Onuchic, 2000).

Here, we report the crystal structure of HiPIP from *T. tepidum* refined at 0.80 Å resolution. *T. tepidum* is a thermophilic photosynthetic purple sulfur bacterium classified in the Chromatiaceae family, which also includes a mesophilic sulfur bacterium, *Allochromatium vinosum*. This HiPIP has 83 amino-acid residues and a redox midpoint potential of +323 mV (Moulis *et al.*, 1993). Its crystal structure has previously been reported at 1.5 Å resolution on the basis of diffraction data collected at room temperature (Nogi, Fathir *et al.*, 2000). We focused our examination on the hydrophobic interaction and crystal packing in this ultrahigh-resolution structure, which led us to discuss the electron-transfer behaviour in comparison with other HiPIP structures.

2. Materials and methods

2.1. Crystallization, data collection and processing

The crystallization method and conditions have been reported previously (Nogi, Kobayashi *et al.*, 2000). The crystallization conditions were optimized by adjustment of the volume ratio of protein to reservoir solution as follows: 5.5 µl of 20% protein solution (in 50 m*M* Tris–HCl pH 8.0) was mixed with 4.5 µl of reservoir solution (1.4 *M* ammonium sulfate and 0.1 *M* sodium citrate pH 3.5) to produce the crystallization drop, which was equilibrated against 1 ml reservoir solution. Plate-like crystals with a maximum size of approximately 0.3 × 0.15 × 0.5 mm were obtained using the sitting-drop vapour-diffusion method at 293 K. Prior to data collection, the crystal was cryoprotected by soaking it in crystallization reservoir solution containing 25% glycerol, mounted in a fibre loop and then frozen to 100 K in a cryogenic nitrogen stream. Diffraction data collection was performed using synchrotron radiation at beamlines BL40B2 and BL44B2 at SPring-8. The best data set (0.80 Å resolution) was collected from a single crystal with a total rotation of 180° and an oscillation step of 1.0° and was recorded on an R-AXIS IV imaging-plate detector at BL40B2. The X-ray wavelength was 0.7293 Å and the crystal-to-detector distance was 110 mm.

Data were processed using *DENZO* and *SCALEPACK* (Otwinowski & Minor, 1997). The unit-cell parameters of the $P2_12_12_1$ crystal were anisotropically much smaller at 100 K [a = 44.697 (1), b = 58.272 (1), c = 23.454 (1) Å] than those determined at room temperature (a = 47.12, b = 59.59, c = 23.62 Å; Nogi, Kobayashi *et al.*, 2000).

2.2. Structural refinement

*SHELX*97 (Sheldrick & Schneider, 1997) and *O* (Jones *et al.*, 1991) programs were used for refinement and model building with manual adjustment, respectively. A randomly selected 3355 reflections (5% of the total observed reflections) in the full resolution range (20–0.80 Å) were used as a test set for free *R*-factor calculation. The 1.5 Å resolution structure at room temperature (Nogi, Fathir *et al.*, 2000) was employed as the initial model for refinement, with all the solvent molecules omitted. With careful consideration of the large changes in unit-cell parameters between room and low temperature, the model was initially relocated in the unit cell with *AMoRe* (Navaza, 1994) and subsequently refined by rigid-body fitting in the resolution range 20–1.5 Å using *SHELX*97, which gave R and $R_{\rm free}$ factors of 0.246 and 0.268, respectively. After checking the map and minor adjustments of the model, several cycles of isotropic refinement in the resolution range 20–0.80 Å lowered R and $R_{\rm free}$ to 0.193 and 0.209, respectively. Thereafter, solvent molecules were automatically introduced to the model structure with *SHELXWAT* (Sheldrick & Schneider, 1997) with a *B*-factor cutoff of 50 Å^2 and sulfate anions were also added manually. At this stage, the R and $R_{\rm free}$ factors were reduced to 0.152 and 0.164, respectively. Further refinement was carried out using conjugate-gradient least-squares minimization with anisotropic *B* factors. In this step, standard deviations of 0.02 and 0.04 Å were used as the restraints for the 1,2 and 1,3 distances and R and $R_{\rm free}$ fell to 0.106 and 0.126, respectively. The H atoms (C—H and N—H) were then located automatically with *SHELX*97, but their coordinates were not refined. The introduction of the H atoms to the model lowered R and $R_{\rm free}$ to 0.100 and 0.115, respectively.

After several cycles of manual adjustment and refinement, multiple conformations of several amino-acid residues and several additional water molecules were added to the model, which was subjected to a final step of one cycle of full-matrix least-squares minimization. In this refinement, the L.S. and BLOC commands were combined to perform the least-squares calculation (Sheldrick & Schneider, 1997). The maximum shifts in atom positions were 0.030 and 0.165 Å and the maximum shifts of the *B* factors were 0.47 and 17.7 Å^2 for non-H atoms and solvent atoms, respectively. The highest and deepest peaks in the final difference map ($F_o - F_c$) were 1.6σ and −1.2σ, respectively. This final model gave R = 0.101 and $R_{\rm free}$ = 0.114. The final model was evaluated with *PROCHECK* (Collaborative Computational Project,

Number 4, 1994). Statistics of the data processing and structure refinement are shown in Table 1.

3. Results and discussion

3.1. Structural model

The structural model of *T. tepidum* HiPIP at 0.80 Å resolution gave *R* factors of 0.101 and 0.092 for all observed and $I > 4(I)$ reflections, respectively. The corresponding $R_{\rm free}$ factors for 3355 randomly selected test-set reflections and for those with $I > 4\sigma(I)$ were 0.114 and 0.103, respectively (Table 1). The model contains all 83 residues, the iron–sulfur cluster, three sulfates and 93 water molecules (seven water molecules were refined with double 'conformations').

The anisotropic temperature factors employed for all atoms, including all solvent atoms, and for alternative conformations of the protein lowered the *R* factors by 4–5%, whereas the positioning of H atoms reduced the *R* factors by ∼0.5%. No H atoms were generated for water molecules, although they could be occasionally identified in the $F_o - F_c$ maps. In the final model, the isotropic *B* factors ranged from 3 to 31 Å^2 and the mean *B* factor was 9.97 Å^2. Eight atoms of the iron–sulfur cluster had a lowest mean *B* factor of 3.25 Å^2 and their maximum shifts in both coordinates and *B* factors were the lowest (<0.001 Å and 0.008 Å^2, respectively) in the last full-matrix least-squares refinement. The root-mean-square (r.m.s.) deviations of the final model from ideal geometry were 0.016 Å and 2.0° for the bond lengths and bond angles, respectively. The stereochemistry check showed that 97.1 and 2.9% of the residues were located in the most favoured and additional allowed regions of the Ramachandran plot, respectively (Table 1).

In contrast to the 1.5 Å resolution structure, the present ultrahigh-resolution structure revealed several multiple side-chain conformations of the residues Pro12, Ile15, Lys25, Pro38 and Ser77. In addition, the solvent molecules and small-molecule ligands appeared much more clearly in the electron-density maps at this resolution (Fig. 2). The 1.5 Å resolution

Table 1
Statistics for data collection, processing and structure refinement.

Data collection and processing	
Unit-cell parameters† (Å)	a = 44.697 (1), b = 58.272 (1), c = 23.454 (1)
Space group	$P2_12_12_1$
Temperature (K)	100
Resolution‡ (Å)	5–0.80 (0.81–0.80)
No. of observed reflections	823255
No. of unique reflections‡	64373 (3094)
Completeness‡ (%)	98.6 (95.5)
$I/\sigma(I)$ (average)‡	27.8 (2.74)
$R_{\rm merge}$ (%)‡	5.2 (39.7)
Structure refinement	
Resolution (Å)	20–0.80
No. of atoms refined	
Protein (non-H)	660
Water (full/partial)	86/7
Sulfate	15
R [$I > 4\sigma(I)$]	0.092
R (all data)	0.101
$R_{\rm free}$ [$I > 4\sigma(I)$]	0.103
$R_{\rm free}$ (all data)	0.114
R.m.s. deviation of bonds (Å)	0.016
R.m.s. deviation of angles (°)	2.0
Average B factors (Å^2)	9.97
Residues in most favoured regions (%)	97.1
Residues in additional allowed regions (%)	2.9

† Estimated standard deviations of the unit-cell parameters are given in parentheses. ‡ Values for the highest resolution shell are given in parentheses.

3.2. Comparison with the 1.5 Å structure

The overall structure has essentially the same fold as the room-temperature structure at 1.5 Å resolution (Nogi, Fathir *et al.*, 2000), but significantly large differences still exist at the C-terminus and in the region around Asp10 (Fig. 1). In the crystal, these two parts contact compactly with the neighbouring molecules. Therefore, these differences have mostly arisen from the effect of cryotemperature on crystal packing in the orientation of the crystallographic *a* axis (Fig. 1), although they may also have been partially affected by the minor adjustment to the crystallization conditions. These differences were also reflected in the large change in the *a* unit-cell parameter (2.42 Å, >5% of *a*) depending on the data-collection temperature. There were no such large changes in the unit-cell parameters of the *b* and *c* axes and also no large structural changes in the direction of the *b* and *c* axes.

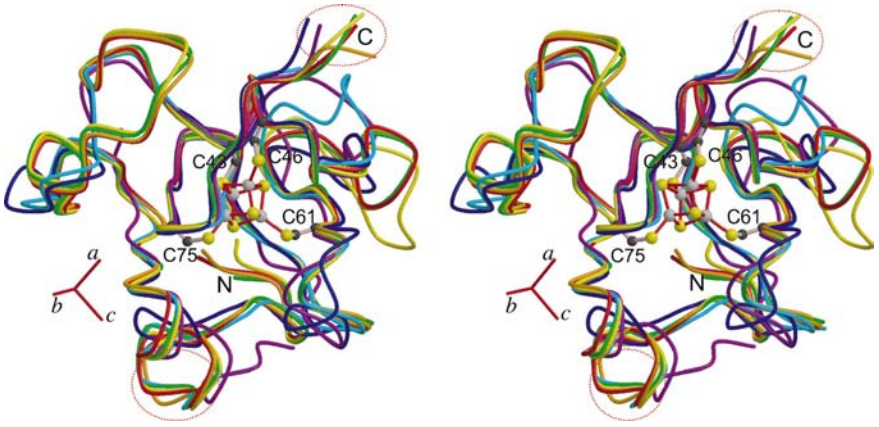

Figure 1
Stereoview of the overall structures of HiPIPs. The folding of HiPIP from *T. tepidum* (red) at 0.8 Å resolution (the present study) is superimposed with those from *T. tepidum* (orange) at 1.5 Å resolution (Nogi, Fathir *et al.*, 2000), *A. vinosum* (yellow) H42Q mutant at 0.93 Å resolution (Parisini *et al.*, 1999), *M. purpuratum* (green) at 2.7 Å resolution (Kerfeld *et al.*, 1998), *H. halophila* (blue) at 2.5 Å resolution (Breiter *et al.*, 1991), *E. vacuolata* (cyan) at 1.8 Å resolution (Benning *et al.*, 1994) and *R. tenius* (purple) at 1.5 Å resolution (Rayment *et al.*, 1992). The unit-cell axes of the crystal of *T. tepidum* HiPIP are indicated. The iron–sulfur cluster with four bridging cysteine residues of *T. tepidum* HiPIP is shown. The relatively large differences between the 0.8 and 1.5 Å structures of *T. tepidum* HiPIP are indicated by red dotted circles. All figures were generated with *MOLSCRIPT* (Kraulis, 1991) and *Raster3D* (Merritt & Bacon, 1997).

structure contained 43 water molecules, whereas 93 molecules were located in the ultrahigh-resolution structure. As shown in Fig. 2(*b*), the electron-density map showed that the geometry around the sulfate ion is essentially tetrahedral. Moreover, most H atoms appeared clearly in the $F_o - F_c$ map at the 3.0σ level, which provides direct evidence for hydrogen bonding. Fig. 2(*c*) show the positioning of the H atoms of Cys75 at the 3.5σ level.

3.3. Comparison of the overall structure of *T. tepidum* HiPIP with other HiPIPs

Although there is considerable variety in the primary structures, redox potentials, net overall charges and sizes of HiPIPs from different species, their iron-cluster structures are highly conserved and the folding in the vicinity of the cluster is very similar (Fig. 1). In addition to the hydrogen bond generated between a backbone N atom (Cys75) and an S atom [(S1)] of the cluster, four other hydrogen bonds between backbone N atoms and S atoms of the cysteinyl ligands are formed in a similar way in all HiPIPs. These hydrogen bonds are thought to be associated with the mid-point redox potential (Low & Hill, 2000). In addition, the aromatic residues responsible for the hydrophobic atmosphere around the cluster are mostly conserved in these HiPIPs. Of the HiPIPs, those from *A. vinosum* and *Marichromatium purpuratum* have the structures closest to that of *T. tepidum*; this is consistent with the high homology among the primary structures of these HiPIPs (Kerfeld *et al.*, 1998; Parisini *et al.*, 1999). These three HiPIPs have relatively close mid-point redox potentials: +323, +350 and +390 mV for *T. tepidum*, *A. vinosum* and *M. purpuratum*, respectively. In contrast, the HiPIPs from *Halorhodospira halophila* and *Rhodocyclus tenius*, which have low sequence homology with that of *T. tepidum*, showed quite large structural differences in the area distant from the cluster. However, the mid-point redox potentials of 310 and 120 mV for the *R. tenius* (Rayment *et al.*, 1992) and *H. halophila* (Breiter *et al.*, 1991) HiPIPs, respectively, do not correspond to these structural differences.

Because the *T. tepidum* HiPIP shows ∼90% sequence homology with the *A. vinosum* HiPIP, it is expected that the structural differences between these two HiPIPs might provide direct insight into the differences between their mid-point redox potentials and their thermal stabilities (Moulis *et al.*, 1993). Superimposition of the C^{α} atoms between the structure of *A. vinosum* HiPIP (the H42Q mutant at 0.93 Å resolution) and the present structure gave an r.m.s. deviation of 0.78 Å. The largest difference in their folding was located between Asn52 and Asp57, which also resulted in one less net overall charge in *T. tepidum* HiPIP (−5) than in *A. vinosum* HiPIP (−6). Despite these differences, a highly conserved iron–sulfur cluster has an approximate C_{2v} point-group symmetry in these two types of HiPIPs, with an r.m.s. deviation of 0.008 Å. In this cluster (Fig. 2*a*), the Fe(1)—Fe(2) distance (2.758 Å) in *T. tepidum* HiPIP is approximately 0.049 Å longer than that of Fe(3)—Fe(4) (2.709 Å), whereas the difference is only 0.025 Å in the structure of *A. vinosum* HiPIP (Table 2). There are no significant differences in the distances of the five conserved hydrogen bonds or in the conformations of the aromatic residues responsible for hydrophobicity around the cluster between these two HiPIPs (Table 2). Thus, the difference in two Fe—Fe bonds between the two clusters, which is relatively small but significant (∼3σ; σ = 0.016 Å for bond lengths, as shown in Table 1), may be primarily responsible for the difference in reduction potential (37 mV); the loop region between Asn52 and Asp57 is distant

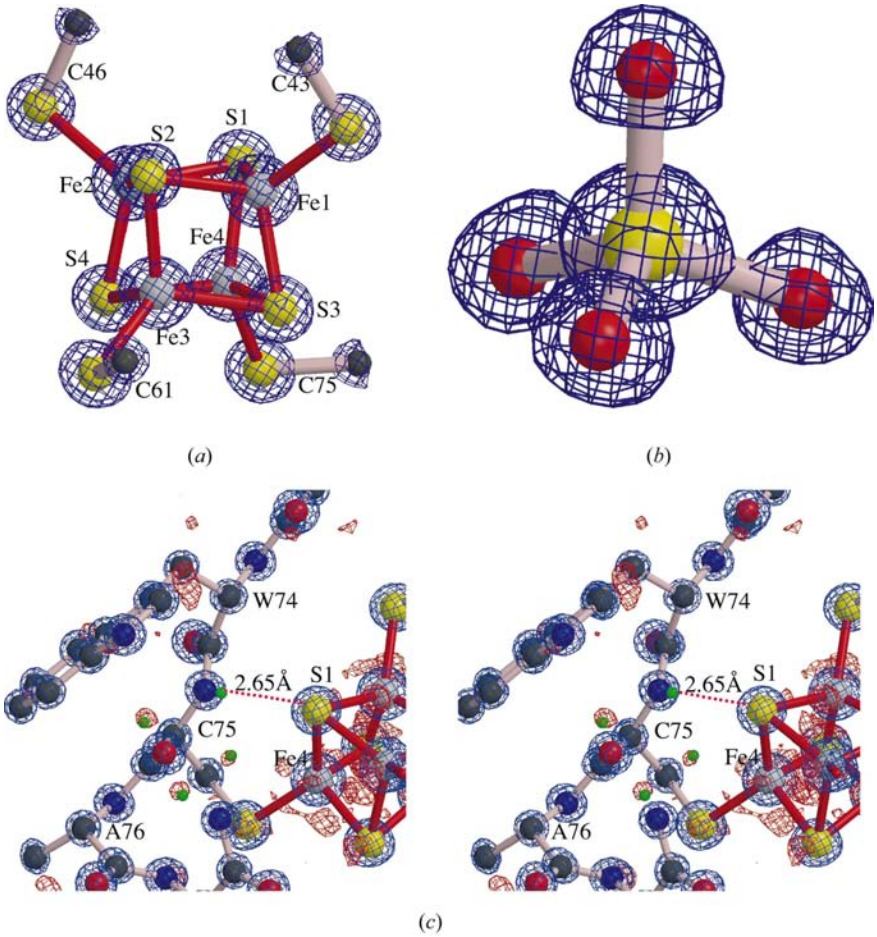

Figure 2
Electron-density maps of *T. tepidum* HiPIP at 0.80 Å resolution. (*a*) $2F_o - F_c$ map of the iron–sulfur cluster contoured at the 10σ level. (*b*) $2F_o - F_c$ map of a sulfate ion contoured at the 5σ level. (*c*) Stereoview of the $2F_o - F_c$ (4σ, blue) and $F_o - F_c$ (3.5σ, red) maps around the Cys75 and Fe(4) apex of the cluster. The predicted positions of the H atoms of Cys75 are shown as green balls and the hydrogen bond between the N atom of Cys75 and S(1) of the cluster is shown as a red dashed line.

from the cluster and has been suggested to be have less relation to the function of HiPIP (Moulis *et al.*, 1993; Nogi, Fathir *et al.*, 2000). Nevertheless, the introduction of one more charged residue and the consequent net overall charge reduction may be connected with the slight increase in the thermal stability of *T. tepidum* HiPIP, as well as the effect of the deletion in the amino-acid sequence.

Table 2
Bond and hydrogen-bond distances in the cluster of *T. tepidum* and *A. vinosum* HiPIPs (Parisini *et al.*, 1999), with estimated standard deviations in parentheses.

Distance (Å)	*T. tepidum*	*A. vinosum*
Covalent bond		
Fe(1)—S(1)	2.316 (2)	2.321 (4)
Fe(1)—S(2)	2.296 (2)	2.292 (5)
Fe(1)—S(3)	2.227 (2)	2.222 (4)
Fe(2)—S(1)	2.299 (2)	2.295 (5)
Fe(2)—S(2)	2.312 (3)	2.310 (4)
Fe(2)—S(4)	2.224 (2)	2.228 (4)
Fe(3)—S(2)	2.243 (2)	2.242 (4)
Fe(3)—S(3)	2.308 (2)	2.306 (4)
Fe(3)—S(4)	2.305 (3)	2.307 (4)
Fe(4)—S(1)	2.271 (2)	2.266 (4)
Fe(4)—S(3)	2.297 (2)	2.295 (4)
Fe(4)—S(4)	2.285 (2)	2.284 (5)
Fe(1)—SG(43)	2.251 (2)	2.252 (4)
Fe(2)—SG(46)	2.275 (2)	2.274 (4)
Fe(3)—SG(61)†	2.257 (2)	2.258 (4)
Fe(4)—SG(75)†	2.262 (2)	2.253 (4)
Metallic bond		
Fe(1)—Fe(3)	2.708 (3)	2.709 (3)
Fe(2)—Fe(4)	2.708 (3)	2.699 (3)
Fe(1)—Fe(4)	2.699 (2)	2.702 (3)
Fe(2)—Fe(3)	2.698 (2)	2.707 (3)
Fe(1)—Fe(2)	2.758 (2)	2.747 (3)
Fe(3)—Fe(4)	2.709 (2)	2.722 (3)
Hydrogen bond		
N(48)—SG(46)	3.448 (5)	3.400 (15)
N(63)—SG(61)†	3.342 (5)	3.351 (11)
N(75)—S(1)†	3.385 (5)	3.396 (12)
N(77)—SG(75)†	3.379 (6)	3.400 (10)
N(79)—SG(46)†	3.495 (6)	3.554 (11)

† Those residues with number (n) larger than 53 have a corresponding number $n + 2$ in *A. vinosum* HiPIP.

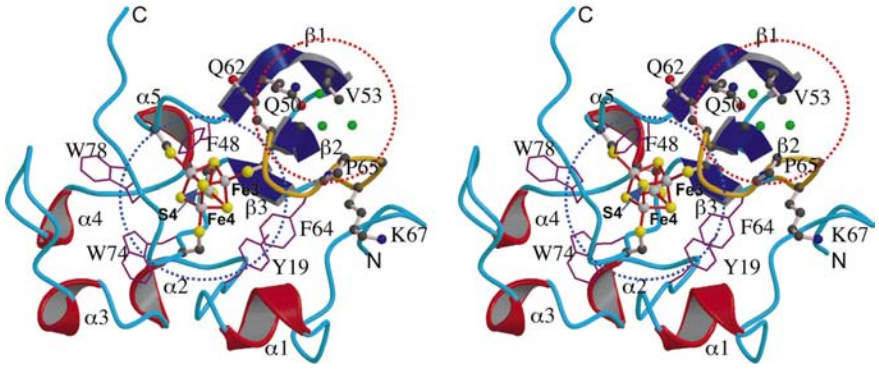

Figure 3
A stereoview of the cavities of *T. tepidum* HiPIP. α-helices (red) and β-strands (blue) are labelled sequentially from the N-teminus to the C-terminus. The side chains of aromatic residues around the cluster are depicted in purple. The hydrophobic cavity is indicated by a blue dashed circle, whereas the partly hydrophobic cavity is indicated by a red dashed circle. In the partly hydrophobic cavity, relevant residues are depicted as ball-and-stick models, the three water molecules are depicted as green balls and the loop is shown in orange.

3.4. Crystal packing and inter-cluster approach distance

The inter-cluster distances are of interest because spectroscopic studies have indicated that the closest distance between the Fe–S clusters is a potential parameter for the intermolecular electron transfer (Dunham *et al.*, 1991; Rayment *et al.*, 1992). In the HiPIP structure, the cluster is surrounded by several conserved aromatic residues that provide a hydrophobic environment (Fig. 3). There is a highly hydrophobic area in the molecular surface in which the S(4) atom of the cluster is located. Because the hydrophobic patch may be of primary importance for the electron transfer and the S(4) atom located at the apex of the 'cubic' cluster can most closely approach the surface, the S(4)—S(4) distance between two neighbouring molecules, as well as the centre-to-centre distance between the clusters, could be considered to be indexes of inter-cluster interaction.

Each asymmetric unit of the present crystal of *T. tepidum* HiPIP contains one protein molecule; the solvent content of the unit cell was previously calculated to be approximately 34% (Matthews, 1968). Each molecule has contacts with 14 other neighbouring molecules when a contact cutoff distance of 5 Å is used between the molecular boundaries in *CNS* (Brünger *et al.*, 1998). In contrast to other HiPIP crystals, in *T. tepidum* HiPIP a closest inter-cluster distance of 23.454 Å (the length of the *c* axis) is observed between two equivalent molecules along the crystallographic *c* axis, in which both centre-to-centre and S(4)—S(4) distances are the same. In this case, the second and third closest inter-cluster distances are 26.2 and 27.0 Å, respectively.

As shown in Table 3, the centre-to-centre inter-cluster distances of all HiPIPs fall in the range 15–25 Å; these values are also less than the maximum distance (25–30 Å) of biological electron transfer *via* quantum tunnelling (Marcus & Sutin, 1985). This distance extends to a wide range in different HiPIPs with various crystal structures and even in the same HiPIP with different packing, although HiPIPs tend to belong to the monoclinic and orthorhombic space groups. Interestingly, the closest inter-cluster distance between neighbouring molecules, a potential indicator of the electron-transfer behaviour (Rayment *et al.*, 1992), does not decrease with the increase in the compactness of the molecular packing in the cell (Table 3). On the contrary, this distance tends to increase with the increase of the packing compactness. In some cases, especially that of an asymmetric unit containing two HiPIP molecules, the inter-cluster interaction is located between the hydrophobic cavities, where the S(4) atom of the cluster is pointed towards the surface of the neighbouring molecule (Rayment *et al.*, 1992; Kerfeld *et al.*, 1998; Parisini *et al.*, 1999). Nevertheless, in the case of relatively compact packing but long inter-cluster

distance, as in the present *T. tepidum* HiPIP, contacts between the two hydrophobic cavities were not observed; in one crystal form of *A. vinosum* HiPIP the S(4)—S(4) distance was even longer than the centre-to-centre distance. These results suggest the inter-cluster distance observed in crystals might be a weak indicator of the possible electron-transfer pathway.

3.5. Structural features and their implications for the HiPIP-related electron-transfer mechanism

Two types of soluble proteins, cytochrome c_2 and HiPIP, are responsible for electron transfer from the cytochrome bc_1 complex to the reaction centre (RC) complex in purple bacteria. HiPIP and cytochrome c_2 interact with the reaction centre by different mechanisms, although the binding regions of the contact proteins overlap for both types of electron carriers. A mechanism based on electrostatic interaction has been well accepted for the cytochrome c_2–RC interaction, whereas a hydrophobic coupling of the encounter surfaces has been suggested for the HiPIP–RC interaction (Osyczka *et al.*, 1998, 2001; Osyczka, Nagashima, Sogabe *et al.*, 1999; Nogi, Fathir *et al.*, 2000). Nevertheless, the role of positively charged lysine residues of HiPIPs must also be considered (Schoepp *et al.*, 1995; Osyczka, Nagashima, Shimada *et al.*, 1999). EPR and NMR studies have shown that HiPIPs might dimerize in the solution through their hydrophobic surfaces, a discovery that has led to important insights regarding the electron-transfer pathway (Groeneveld *et al.*, 1988; Bertini *et al.*, 1993; Couture *et al.*, 1999). These spectroscopic results indicated that the exchange constant in the potential dimer in solution was basically independent of the ionic strength, but that the HiPIP–RC interaction was significantly related to the ionic strength, which implies that the hydrophobic surface might not be simply equated with the electron-transfer path.

Although a *T. tepidum* HiPIP molecule is surrounded by many other molecules in crystals, there are several areas on its molecular surface that are inaccessible to other protein molecules. These areas are mostly located in the proximal and distal sides of the cluster, as shown in Fig. 3. It has been shown that these two areas of the molecular surface have very different electrostatic potentials: the proximal side is highly hydrophobic, while the distal side is hydrophilic (Nogi, Fathir *et al.*, 2000). From analysis using *VOIDOO* (Kleywegt & Jones, 1994), the hydrophobic proximal side was shown to have a cavity where the S(4) atom at an apex of the cubic cluster approaches the hydrophobic surface. The present ultrahigh-resolution structure in which the H atoms could be located revealed that another cavity that is partly hydrophobic and uncharged is located near the Fe(3) atom of the cluster (Fig. 3). This cavity is relatively small and is mostly constructed of β-strands and a loop composed of residues Gln50, Val53, Gly60-Cys61-Gln62 and Phe64-Pro65-Gly66-Lys67. This region includes a few hydrophilic residues, but no charged residues except Lys67. The positively charged side chain of the exceptional Lys67 is far from the cavity, supporting the partial hydrophobic atmosphere in this region. Three water molecules are found in this cavity and no neighbouring protein molecules accessible to this region are found in the crystal packing.

Table 3
Crystal packing and inter-cluster distances in HiPIPs.

Species	Space group	Solvent content† (%)	Inter-cluster distances (Å)		PDB code
			Centre–centre	S(4)–S(4)	
A. vinosum	$P2_1$	30	24.4	23.9	1hip
A. vinosum	$P2_12_12_1$	30	24.6	22.9	1boy
T. tepidum	$P2_12_12_1$	34	23.5	23.5	1iua
M. purpuratum	$P2_12_12$	34	16.5	12.6/13.9‡	3hip
R. tenius	$P2_1$	40	15.4	10.9	1isu
A. vinosum	$P2_12_12_1$	45	16.7	18.2	1cku
E. vacuolata	$C222_1$	48	19.2	17.5	1hpi
H. halophila	$P2_1$	50	16.9	13.4	2hip
A. vinosum	$I2_13$	70	22.2	?	?

† The species in this table were listed in increasing order of solvent-content percentage. ‡ This second value (13.9) was reported previously (Kerfeld *et al.*, 1998), and might not be the closest value.

Although the main hydrophobic cavity was previously thought to be of primary importance, the special location of this partly hydrophobic cavity may suggest a role in electron transfer. Firstly, the bottom of the cavity is Cys61, which co-ordinates with the Fe(3) atom of the cluster. Both experimental and theoretical studies have revealed there to be a total of one iron pair, with mixed valences of +2.5 for each iron, and that there was possibly an equilibrium of the distribution between the Fe(4)–Fe(3) and Fe(3)–Fe(2) pairs that share the mixed valence (Bertini *et al.*, 1993, 1995). In this equilibrium, Fe(3) always seems to have a valence of +2.5, suggesting that this iron plays some special role. In other words, the interaction between this cavity and Fe(3) through Cys61 may contribute to part of the electron-transfer pathway. Secondly, this cavity is located near the main hydrophobic cavity and has some hydrophilic residues but no charged residues. An exception is that one lysine residue (Lys67) contributes its main-chain part to this cavity; its side chain, however, is distant from the cavity (Fig. 3). Nevertheless, this lysine may play a significant role in HiPIP–RC recognition (Schoepp *et al.*, 1998). Thus, this partly hydrophobic structure supports the hydrophobic patch for electron transfer through this region and, more importantly, might help to explain the fact that mutations at the potential encounter position on the reaction centre, consisting of a change from hydrophobic (valine) or negatively charged residues (glutamates) to positively charged residues (lysine), significantly decreased the electron-transfer efficiency of HiPIP (Osyczka, Nagashima, Shimada *et al.*, 1999).

The authors would like to thank Drs K. Miura and S. Adachi of SPring-8, Japan for X-ray diffraction data collection (at BL40B2 by the proposal 2001A0163-NL-np and BL44B2). This work was supported in part by the 'Research for the Future' Program (JSPS-RFTF 97L00501 to KM) from the Japan Society for the Promotion of Science.

References

Agarwal, A., Li, D. & Cowan, J. A. (1995). *Proc. Natl Acad. Sci. USA*, **92**, 9440–9444.

Balabin, I. A. & Onuchic, J. N. (2000). *Science*, **290**, 114–117.

Banci, L., Bertini, I., Carloni, P., Luchinat, C. & Orioli, P. L. (1992). *J. Am. Chem. Soc.* **114**, 10683–10689.

Bartsch, R. G. (1978). *Methods Enzymol.* **53**, 329–340.

Benning, M. M., Meyer, T. E., Rayment, I. & Holden, H. M. (1994). *Biochemistry*, **33**, 2476–2483.

Bertini, I., Capozzi, F., Eltis, L. D., Fello, I. C., Luchinat, C. & Picconi, M. (1995). *Inorg. Chem.* **34**, 2516–2523.

Bertini, I., Gaudemer, A., Luchinat, C. & Piccioli, M. (1993). *Biochemistry*, **32**, 12887–12893.

Breiter, D. R., Meyer, T. E., Rayment, I. & Holden, H. M. (1991). *J. Biol. Chem.* **266**, 18660–18667.

Brünger, A. T., Adams, P. D., Clore, G. M., DeLano, W. L., Gros, P., Grosse-Kunstleve, R. W., Jiang, J. S., Kuszewski, J., Nilges, M., Pannu, N. S., Read, R. J., Rice, L. M., Simonson, T. & Warren, G. L. (1998). *Acta Cryst.* D**54**, 905–921.

Carter, C. W. Jr, Kraut, J., Freer, S. T., Alden, R. A., Sieker, L. C., Adman, E. & Jensen, L. H. (1972). *Proc. Natl Acad. Sci. USA*, **69**, 3526–3529.

Collaborative Computational Project, Number 4 (1994). *Acta Cryst.* D**50**, 760–763.

Couture, M. M.-J., Auger, M., Rosell, F., Mauk, A. G., Boubour, E., Lennox, R. B. & Eltis, L. D. (1999). *Biochim. Biophys. Acta*, **1433**, 159–169.

Dunham, W. R., Hagen, W. R., Fee, J. A., Sands, R. H., Dunbar, J. B. & Humblet, C. (1991). *Biochim. Biophys. Acta*, **1079**, 253–262.

Glaser, T., Bertini, I., Moura, J. J. G., Hedman, B., Hodgson, K. O. & Solomon, E. I. (2001). *J. Am. Chem. Soc.* **123**, 4859–4860.

Groeneveld, C. M., Ouwerling, M. C., Erhelens, C. & Canters, G. W. (1988). *J. Mol. Biol.* **200**, 189–199.

Jones, T. A., Zou, J. Y., Cowan, S. W. & Kjeldgaard, M. (1991). *Acta Cryst.* A**47**, 110–119.

Kerfeld, C. A., Salmeen, A. E. & Yeates, T. O. (1998). *Biochemistry*, **37**, 13911–13917.

Kleywegt, G. J. & Jones, T. A. (1994). *Acta Cryst.* D**50**, 178–185.

Kraulis, P. J. (1991). *J. Appl. Cryst.* **24**, 946–950.

Low, D. W. & Hill, M. G. (2000). *J. Am. Chem. Soc.* **122**, 11039–11040.

Marcus, R. A. & Sutin, N. (1985). *Biochim. Biophys. Acta*, **811**, 265–316.

Matthews, B. W. (1968). *J. Mol. Biol.* **33**, 491–497.

Merritt, E. A. & Bacon, D. J. (1997). *Methods Enzymol.* **277**, 505–524.

Meyer, T. E., Przysiecki, C. T., Watkins, J. A., Bhattacharyya, A., Simondsen, R. P., Cusanovich, M. A. & Tollin, G. (1983). *Proc. Natl Acad. Sci. USA*, **80**, 6740–6744.

Moulis, J.-M., Scherrer, N., Gagnon, J., Rofest, E., Petillot, Y. & Garcia, D. (1993). *Arch. Biochem. Biophys.* **305**, 186–192.

Navaza, J. (1994). *Acta Cryst.* A**50**, 157–163.

Nogi, T., Fathir, I., Kobayashi, M., Nozawa, T. & Miki, K. (2000). *Proc. Natl Acad. Sci. USA*, **97**, 13561–13566.

Nogi, T., Kobayashi, M., Nozawa, T. & Miki, K. (2000). *Acta Cryst.* D**56**, 656–658.

Osyczka, A., Nagashima, K. V. P., Shimada, K. & Matsuura, K. (1999). *Biochemistry*, **38**, 2861–2865.

Osyczka, A., Nagashima, K. V. P., Sogabe, S., Miki, K., Shimada, K. & Matsuura, K. (1999). *Biochemistry*, **38**, 15779–15790.

Osyczka, A., Nagashima, K. V. P., Sogabe, S., Miki, K., Shimada, K. & Matsuura, K. (2001). *J. Biol. Chem.* **276**, 24108–24112.

Osyczka, A., Nagashima, K. V. P., Sogabe, S., Miki, K., Yoshida, M., Shimada, K. & Matsuura, K. (1998). *Biochemistry*, **37**, 11732–11744.

Otwinowski, Z. & Minor, W. (1997). *Methods Enzymol.* **276**, 307–326.

Parisini, E., Capozzi, F., Lubini, P., Lamzin, V., Luchinat, C. & Sheldrick, G. M. (1999). *Acta Cryst.* D**55**, 1773–1784.

Rayment, I., Wesenberg, G., Meyer, T. E., Cusanovich, M. A. & Holden, H. M. (1992). *J. Mol. Biol.* **228**, 672–686.

Schoepp, B., Parot, P., Menin, L., Gaillard, J., Richaud, P. & Vermeglio, A. (1995). *Biochemistry*, **34**, 11736–11742.

Sheldrick, G. M. & Schneider, T. R. (1997). *Methods Enzymol.* **227**, 319–343.

Soriano, A., Li, D., Bian, S., Agarwal, A. & Cowan, J. A. (1996). *Biochemistry*, **35**, 12479–12486.